

Defect-induced spin textures in magnetic solids

M. E. Zhitomirsky

*Université Grenoble Alpes, CEA, IRIG, PHELIQS, 38000 Grenoble, France and
Institut Laue-Langevin, 71 avenue des Martyrs, 38042 Grenoble, France*

Vijay B. Shenoy

*Centre for Condensed Matter Theory, Department of Physics,
Indian Institute of Science, Bangalore 560 012, India*

R. Moessner

*Max-Planck-Institut für Physik Komplexer Systeme,
Nöthnitzer Straße 38, D-01187 Dresden, Germany*

(Dated: December 3, 2024)

We investigate spin textures induced by nonmagnetic vacancies in classical noncollinear magnets. By developing an “elasticity theory” for spin systems, we show that a defect-induced spin readjustment decays with a power law at large distances. The power-law exponent depends on the multipole moment of the local spin deformation, which is in turn determined by both the lattice symmetry and the equilibrium spin configuration in the absence of a defect. The interplay of these two ingredients is best illustrated by the J_1 - J_2 Heisenberg model on a kagome lattice for which a point vacancy may produce spin deformations that decay as $1/r^2$ for the $q = 0$ ground state and as a $1/r$ for the $\sqrt{3} \times \sqrt{3}$ magnetic structure. The analytic conclusions are confirmed by extensive numerical simulations. We also compute the fractional magnetic moments associated with vacancies and other lattice defects. Our results shed light on relative fragility of different magnetic structures with respect to spin glass formation at higher doping levels.

I. INTRODUCTION

The role of structural disorder is a recurring theme in experimental studies of magnetic materials, see [1–15]. It is now widely recognized that disorder is not only a source of unwanted or parasitic effects but may also produce interesting physics and enable various applications [16–18]. Early theoretical studies on defect-induced phenomena in magnetically ordered crystals date back more than half a century, see the articles by de Gennes [19], Villain [20] and references therein. The discovery of high-temperature superconductivity in doped antiferromagnets gave a new impetus to theoretical studies [21–26]. More recently, the effect of structural disorder was investigated for geometrically frustrated magnets and related systems with extra ‘accidental’ degeneracies among classical ground states. Random impurities and bond defects can lower the energy of certain ordered spin configurations providing instances of order from disorder selection [27–34]. Alternatively, if the classical degeneracy is high, randomness in the magnetic Hamiltonian may induce either a spin glass state [35–38] or various kinds of quantum and classical spin liquids [39–44]. In addition, considerable attention was devoted to properties of an isolated impurity (vacancy) in ordered and disordered antiferromagnets [45–59]. At low temperatures, nonmagnetic vacancies can generate effective paramagnetic moments, which can in turn acquire fractional values [52, 53, 55, 56].

A physical phenomenon common to many theoretical and experimental works is the local spin readjustment, or canting, in the vicinity of a structural defect. For magnets with spontaneously broken continuous symme-

tries, the resulting spin textures can extend over large distances. Such clouds of canted spins surrounding nonmagnetic defects have a strong effect on various physical properties including magnon transport and stability of magnetic structures with respect to transformation into a spin glass state upon increasing the density of defects. Taking into account importance of spin currents for spintronics applications [60] and also a general interest in the role of defects in magnets, we revisit in our work the problem of strain fields created by isolated defects in ordered magnetic structures.

The spin canting induced by a single defect bond is well understood, see [20–24] and discussion in Sec. II. The associated strain field propagates with distance r from the defect as $1/r^{D-1}$ both for two ($D = 2$) and three ($D = 3$) dimensional lattices. However, a consistent description of spin textures near a spin vacancy in a noncollinear antiferromagnet is still lacking. A number of published papers have proposed different distance dependence, such as the $1/r^D$ law [39, 54] or the $1/r^{D+1}$ law [53], both of which supported by the numerical results. In essence, the available results imply that dimensionality alone is not sufficient to determine the asymptotic behavior of the strain field induced by a nonmagnetic vacancy.

We demonstrate below that the decay law also depends on *symmetry* of an unperturbed magnetic structure. We base our consideration on the elasticity approach to ordered magnetic states. This provides a simple analytic description for the spin canting far away from the defects. Our analytic predictions are confirmed by numerical results.

II. COPLANAR SPIN TEXTURES

A. Analytic theory

We consider the classical Heisenberg model on a regular lattice with unit-length spins $|\mathbf{S}_i| = 1$:

$$\hat{\mathcal{H}} = \sum_{\langle ij \rangle} J_{ij} \mathbf{S}_i \cdot \mathbf{S}_j, \quad (1)$$

where summation is taken over bonds. A noncollinear magnetic state may appear as a result of competing exchange interactions.

We first address the case that the lowest energy structure is a *coplanar* spin spiral. There are notable exceptions to this, *e.g.*, [61], and we will be addressing the fully non-collinear case in the next section. We choose the x - z plane as the rotation plane for spins:

$$\mathbf{S}_i^{(0)} = (\sin \theta_i, 0, \cos \theta_i). \quad (2)$$

A lattice defect modifies locally the interaction parameters in the Hamiltonian (1) causing readjustment of surrounding spins or, equivalently, a strain in the magnetic structure. The early works have focused on the problem of a defect antiferromagnetic bond in a collinear ferromagnet [20–26]. Once the strength of a perturbed bond exceeds a threshold value, a canted spin state arises in the vicinity of the defect, with a slowly decaying long-range tail. For a defect in a noncollinear antiferromagnet, spins begin to readjust for an arbitrarily weak modification of the perturbed bond(s). The deformation field \mathbf{m}_i can be defined as

$$\mathbf{m}_i = \mathbf{S}_i - \mathbf{S}_i^{(0)}, \quad (3)$$

where \mathbf{S}_i is the actual spin orientation on a site i and $|\mathbf{m}_i| \rightarrow 0$ at large distances.

In order to obtain the equation for \mathbf{m}_i , we transform to the rotating frame such that the local \mathbf{z}_i axis points along $\mathbf{S}_i^{(0)}$ and the \mathbf{x}_i axis lies in the helix plane. The energy (1) transforms to

$$E = \sum_{\langle ij \rangle} J_{ij} [m_i^y m_j^y + \cos \theta_{ij} (S_i^z S_j^z + m_i^x m_j^x) + \sin \theta_{ij} (S_i^z m_j^x - m_i^x S_j^z)], \quad (4)$$

with $\theta_{ij} = \theta_i - \theta_j$ and $S_i^z = \sqrt{1 - m_i^x{}^2 - m_i^y{}^2}$.

The linear terms in the energy functional $E(\mathbf{m}_i)$ are explicitly given by

$$E_1 = - \sum_i m_i^x h_i, \quad h_i = \sum_j J_{ij} \sin \theta_{ij}. \quad (5)$$

Here, h_i is an in-plane component of a magnetic torque acting on a single spin. For sites outside the defect region

$h_i \equiv 0$. Expanding S_i^z to the second order in m_i^α we obtain the strain energy as

$$E_2 = \sum_{\langle ij \rangle} J_{ij} \left\{ -\frac{1}{2} \cos \theta_{ij} [(m_j^x - m_i^x)^2 + (m_j^y - m_i^y)^2] + m_i^y m_j^y (1 - \cos \theta_{ij}) \right\}, \quad (6)$$

which is a positively defined quadratic form.

A lattice defect exerts a torque on adjacent spins: $h_i \neq 0$. This, in turn, produces a distribution of m_i^α away from the defect. To proceed analytically, we initially assume that the perturbation is weak $|\mathbf{h}_i| \ll |J_{ij}|$. In addition, the calculation is performed for a spin spiral $\theta_i = \mathbf{Q} \cdot \mathbf{r}_i$ with the wave vector \mathbf{Q} corresponding to the minimum of the Fourier transform of the exchange matrix

$$J_{\mathbf{q}} = \sum_j J_{ij} e^{i\mathbf{Q} \cdot \mathbf{r}_{ij}}. \quad (7)$$

Minimization of $E_1 + E_2$ yields the following equations for two components of the deformation field:

$$\begin{aligned} \sum_j J_{ij} \cos(\mathbf{Q} \cdot \mathbf{r}_{ij}) m_j^x - J_{\mathbf{Q}} m_i^x &= h_i^x, \\ \sum_j J_{ij} m_j^y - J_{\mathbf{Q}} m_i^y &= h_i^y. \end{aligned} \quad (8)$$

For a magnetic spiral, defect bonds or vacancies produce no h_i^y . Still, we may consider a general perturbation with a finite h_i^y . Solutions to the above equations are straightforwardly expressed in terms of the lattice Green's functions [62]:

$$\begin{aligned} m_i^x &= \frac{1}{N} \sum_{\mathbf{k}} \sum_j \frac{e^{i\mathbf{k}(\mathbf{r}_i - \mathbf{r}_j)}}{\frac{1}{2}(J_{\mathbf{k}+\mathbf{Q}} + J_{\mathbf{k}-\mathbf{Q}}) - J_{\mathbf{Q}}} h_j^x, \\ m_i^y &= \frac{1}{N} \sum_{\mathbf{k}} \sum_j \frac{e^{i\mathbf{k}(\mathbf{r}_i - \mathbf{r}_j)}}{J_{\mathbf{k}} - J_{\mathbf{Q}}} h_j^y. \end{aligned} \quad (9)$$

At large distances, the phase factors rapidly oscillate and the momentum sums are dominated by small momenta. Expanding the denominators we obtain asymptotically

$$\begin{aligned} m_i^x &\approx \frac{1}{N} \sum_{\mathbf{k}} \frac{e^{i\mathbf{k}\mathbf{r}_i}}{a^2 |\mathbf{k}|^2} \sum_j h_j^x e^{-i\mathbf{k}\mathbf{r}_j}, \\ m_i^y &\approx \frac{1}{N} \sum_{\mathbf{k}} \frac{e^{i\mathbf{k}\mathbf{r}_i}}{\lambda^2 + b^2 |\mathbf{k}|^2} \sum_j h_j^y e^{-i\mathbf{k}\mathbf{r}_j}, \end{aligned} \quad (10)$$

where $\lambda^2 = J_0 - J_{\mathbf{Q}}$, $a^2 = \frac{1}{2} J''_{\mathbf{Q}}$, and $b^2 = \frac{1}{2} J''_0$. Because of 'a gap' $\lambda > 0$, the out-of-plane components m_i^y are short-ranged and decay exponentially with distance. The in-plane distortion of spins m_i^x exhibits instead a slower power-law dependence at large distances. The asymptotic form of m_i^x (10) follows from a solution of the Laplace's equation written in Fourier transformed

form. Its real space behavior is determined by a small $|\mathbf{k}|$ expansion of the torque source

$$\hat{Q}(\mathbf{k}) = \sum_j h_j^x e^{-i\mathbf{k}\mathbf{r}_j}, \quad (11)$$

which is analogous to the multipole expansion for a system of point charges.

If a local perturbation is not infinitesimally weak, one generally needs to solve a nonlinear lattice problem based on the full energy (4). Still, the quadratic approximation (6) is valid at large distances, where the spin tilting is small. Replacing \mathbf{m}_i with a continuous field $\mathbf{m}(\mathbf{r})$ one obtains a gradient expansion for the strain energy

$$E = \int d^D r \left[K_x (\nabla m^x)^2 + K_y (\nabla m^y)^2 + \lambda^2 m^y{}^2 \right]. \quad (12)$$

The in-plane spin readjustment described by an angle $\phi(\mathbf{r}) \approx m^x(\mathbf{r})$ satisfies the Laplace's equation

$$\Delta\phi = 0. \quad (13)$$

Its solution corresponds to an ‘electric’ potential field produced by a delta-like source term. The source term can be still found from Eqs. (5) and (11), but its amplitude becomes renormalized by nonlinear corrections.

As an example, let us consider a bond defect that connects sites i' and j' with a distinct exchange coupling \tilde{J} , which differs by $\delta J = \tilde{J} - J_{ij}$ from the corresponding value in the surrounding lattice. The produced source term has a dipole symmetry, since the function h_i in Eq. (5) changes sign under the permutation $i \leftrightarrow j$. Hence, a bond defect generates a readjustment of spins in the form of a dipole potential [20]

$$\phi(\mathbf{r}) = \frac{\mathbf{d} \cdot \mathbf{r}}{r^D} = \frac{d^\alpha \hat{r}^\alpha}{r^{D-1}}, \quad (14)$$

where $\hat{\mathbf{r}} = \mathbf{r}/r$. The dipole moment \mathbf{d} is parallel to the modified bond $\mathbf{d} \parallel \mathbf{r}_{i'j'}$ and in the linear approximation $|\mathbf{d}| \sim |\delta J|$. In two and three dimensions, magnetic distortions slowly decay with distance as $1/r$ and $1/r^2$, respectively. Obviously, the power law behavior for $\phi(\mathbf{r})$ is related to the Goldstone mode for global rotations of the coplanar magnetic structure about the orthogonal axis.

Let us now investigate the effect of a vacancy. Instead of removing a spin, the vacancy can be modeled by gradually weakening the surrounding bonds. Therefore, the ‘bond-defect’ theory is fully adaptable to this case as well. The torque applied to the adjacent spins can be calculated directly from Eq. (5). In the linear approximation $\phi_i \propto h_i$, hence, one can deduce the leading multipole moment that appears in Eqs. (10) and (11) from a pictorial representation of the spin canting in the nearest-neighbor shell. Figure 1 illustrates the corresponding spin readjustment for four representative examples.

We begin with the Heisenberg triangular antiferromagnet (TAF), Fig. 1(a). Due to geometric magnetic frustration, antiparallel alignment of spins cannot be simultaneously achieved for all nearest-neighbor bonds, and

the lowest energy spin configuration corresponds to the 120° magnetic structure. This magnetic structure is an example of a magnetic spiral with the ordering wave vector $\mathbf{Q} = (4\pi/3, 0)$, where the nearest-neighbor distance is used as a unit length.

A lattice vacancy relieves frustration in the surrounding triangular plaquettes and allows for the adjacent spins to align more antiparallel to each other. The associated spin tilting alternates around the vacant site as shown in Fig. 1(a) with $\phi_i, h_i \sim \cos 3\varphi$, where φ is the azimuthal angle. Thus, the multipole expansion for the torque produced by a vacancy in TAF starts with an octupole term $T^{\alpha\beta\gamma} = \sum_i h_i r_i^\alpha r_i^\beta r_i^\gamma$. The induced spin texture varies at large distances as

$$\phi(\mathbf{r}) \propto \frac{\text{Re}(\hat{x} + i\hat{y})^3}{r^{D+1}} \quad (15)$$

corresponding to the $1/r^3$ law in two dimensions. A spin texture created around a vacancy in TAF possesses three-fold rotation symmetry. In particular, spins do not tilt along the vertical line and two other equivalent crystallographic directions passing through the vacant site. These directions correspond to zeros of the octupole harmonic and all higher-order terms that are present in the multipole expansion.

The second model is the frustrated square lattice antiferromagnet (FSAF) with nearest J_1 and next-nearest J_2 neighbor Heisenberg exchange interactions. For $J_2 > \frac{1}{2}J_1$ the ordering wave vector is either $\mathbf{Q} = (\pi, 0)$ or $\mathbf{Q} = (0, \pi)$ and the model has degenerate classical ground states. The degeneracy can be visualized as an arbitrary mutual orientation of two interpenetrating square lattice antiferromagnets formed by the diagonal J_2 bonds. At zero temperature, a vacancy enforces an orthogonal orientation of the two interpenetrating antiferromagnetic sublattices [27]. The resulting spin readjustments in the nearest-neighbor shell $\phi_i, h_i \sim \cos 2\varphi$, see Fig. 1(b), is described by a nonzero quadrupole moment $Q^{\alpha\beta} = \sum_i h_i r_i^\alpha r_i^\beta$. The long-distance behavior of magnetic distortions in this case is given by

$$\phi(\mathbf{r}) \propto \frac{\text{Re}(\hat{x} + i\hat{y})^2}{r^D}, \quad (16)$$

which is slower than for the TAF. Spins along the nodal directions of the quadrupole moment do not tilt away from their initial orientations irrespective of the distance to the vacancy.

The next two examples illustrated in Figs. 1(c) and 1(d) correspond to the J_1 - J_2 Heisenberg antiferromagnet on a kagome lattice (KAF). The nearest-neighbor Heisenberg antiferromagnet with $J_1 > 0$ and $J_2 = 0$ has an extensive degeneracy of the classical ground states. For any triangular plaquette, any three spins are constrained to form a 120° configuration. However, this does not fix a periodicity of the magnetic structure [63–65]. The second-neighbor exchange J_2 lifts this macroscopic degeneracy in two different ways depending on its sign.

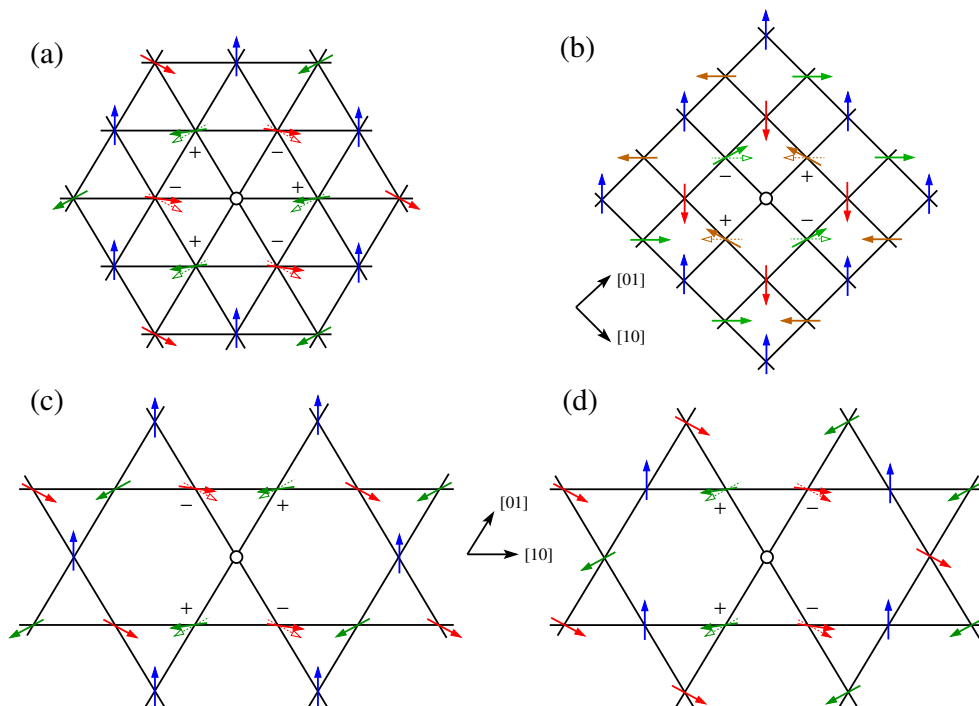


FIG. 1. Magnetic structure distortions near a nonmagnetic vacancy (white circle) in noncollinear antiferromagnets. The torque sign or the spin tilting direction is indicated by $+/-$ for the nearest spins around the vacancy. (a) Triangular antiferromagnet; (b) J_1 - J_2 square-lattice antiferromagnet with $J_2 > 0.5J_1$; (c) the $q = 0$ state for J_1 - J_2 kagome antiferromagnet ($J_2 > 0$) and (d) the $\sqrt{3} \times \sqrt{3}$ structure ($J_2 < 0$).

For $J_2 > 0$, the $q = 0$ state becomes energetically stable, Fig. 1(c), whereas $J_2 < 0$ selects the $\sqrt{3} \times \sqrt{3}$ magnetic structure, Fig. 1(d), [64]. Having different translational patterns, the two states also differ in the sense of spin rotations described by their chirality. The $q = 0$ state exhibits the same chirality for all triangular plaquettes, whereas in the $\sqrt{3} \times \sqrt{3}$ structure the chiralities for up and down plaquettes have opposite signs.

A spin removal produces local distortions with different symmetry in the two classical ground states of KAF. This can be traced back to the presence of $\sin \theta_{ij}$ in the expression for torque (5), which in turn depends on the chirality pattern. For the $q = 0$ state, the perturbation around a vacancy has a quadrupolar symmetry, Fig. 1(c), whereas for the $\sqrt{3} \times \sqrt{3}$ state the perturbation is of the dipolar type, Fig. 1(d). Hence, long-distance asymptotes are different for the vacancy-induced spin textures in the two states: $1/r^2$ for the $q = 0$ magnetic structure and $1/r$ for the $\sqrt{3} \times \sqrt{3}$ state. There is also an essential difference between the quadrupole spin textures in Figs. 1(b) and 1(c). A local site symmetry for a kagome lattice is D_2 as opposed to D_4 for a square lattice. As a result, absence of spin tilting along the nodal directions of the quadrupole moment is not symmetry protected for the $q = 0$ state of KAF. Spins in the horizontal [10] chains of a kagome lattice, Fig. 1(c), readjust, though, with a faster $1/r^3$ decay law, which is determined by the sub-leading octupole term in the multipole expansion of the

vacancy torque. Such a term is excluded by symmetry for FSAFM, Fig. 1(b).

The slow $1/r$ decay of spin distortions is also characteristic for incommensurate helical structures. An example of such a system is an orthorhombically distorted TAF with different strength of exchange interactions in the horizontal chains (J) and on the interchain zigzag bonds (J'). The pattern of tilting angles produced by a vacant site is still given by Fig. 1(a), but the amplitudes ϕ_i are now different for the horizontal chain that includes a vacancy and for the adjacent horizontal chains. The source term in Eq. (11) has a lower dipole symmetry and, consequently, magnetic distortions decrease with distance as $1/r$, that is much slower than $1/r^3$ dependence found for TAF.

B. Numerical results

A classical spin configuration minimizes the exchange energy (1) under the condition

$$\mathbf{S}_i = \frac{\mathbf{h}_i}{|\mathbf{h}_i|}, \quad \mathbf{h}_i = \sum_j J_{ij} \mathbf{S}_j. \quad (17)$$

We solve the resulting system of equations iteratively on periodic clusters with linear sizes up to $L = 10^3$ unit cells for 2D lattices and $L = 10^2$ for 3D lattices. The iteration procedure consists of sequential rotations of spins

towards the instantaneous local fields until the stationary state is reached. To initiate the process we have used either a fully ordered spin state or multiple random configurations. In the latter case the state with the lowest final energy was kept and compared with the structure obtained from the ordered configuration to make sure that the results are the same. Numerical data are shown for distances $r < L/2$, where the finite-size effects are small. Distances are measured in the units of the nearest-neighbor spacing between spins.

Figure 2(a) compares the decay of vacancy-induced spin distortions for three two-dimensional frustrated Heisenberg antiferromagnets: on a triangular lattice, on a square lattice with a diagonal exchange $J_2 = J_1$, and on a distorted triangular lattice with $J' = 0.518J$, which corresponds to an incommensurate spiral described by the wave vector $\mathbf{Q} = (7\pi/6, 0)$. The deviation angle $\phi(r)$ is shown for spins on the radial chains passing through the vacancy and parallel to the [10] crystallographic direction, see Fig. 1. For FSAF, the spin distortions have different magnitudes on the two interpenetrating $\sqrt{2} \times \sqrt{2}$ sublattices and we show results only for one of them. For both sublattices the power law decay occurs with the exponent $n = 2$. In TAF, $\phi(r)$ decreases considerably faster with the power law exponent $n = 3$. However, once the triangular lattice is orthorhombically distorted, the spin texture extends to much larger distances and the power law exponent changes to $n = 1$.

Next we consider the J_1 - J_2 Heisenberg antiferromagnet on a kagome lattice fixing $J_2/J_1 = \pm 0.1$ to stabilize either the $q = 0$ or the $\sqrt{3} \times \sqrt{3}$ structures, respectively. A vacancy in the $\sqrt{3} \times \sqrt{3}$ state produces the deformation field with the dipole symmetry. Numerical results in Fig. 2(b) illustrate the corresponding $1/r$ decay for spin deviations along the [01] chain, which goes through the vacancy site, and along the horizontal [10] chain, which passes through the base of the triangular plaquette containing the vacancy, see Fig. 1(d). For both chain directions the power law exponent is the same $n = 1$.

Similar results for the $q = 0$ state show a faster power-law decay of spin deviations with distinct exponents $n = 2$ and 3 for the two chosen lines. The $n = 2$ exponent for the [01] chain fully agrees with the quadrupole deformation field (16). On the other hand, the horizontal [10] line corresponds to a nodal direction of the quadrupole moment. Hence, as was argued in Sec. IIA, the spin canting angle along this line is determined at large distances by the subleading octupole term. The different vacancy response of the two coplanar 120° states of the kagome antiferromagnet may lead to their strikingly different stability under the doping. This interesting question deserves further investigation.

The bottom panel in Fig. 2(c) shows numerical results for a few three-dimensional spin models. The first example is the layered TAF with an interlayer coupling taken as $J_c = J$ for an illustration. The pattern of local spin distortions remain the same as in 2D, Fig. 1(a), irrespective of the sign of interplane coupling. Hence, spin dis-

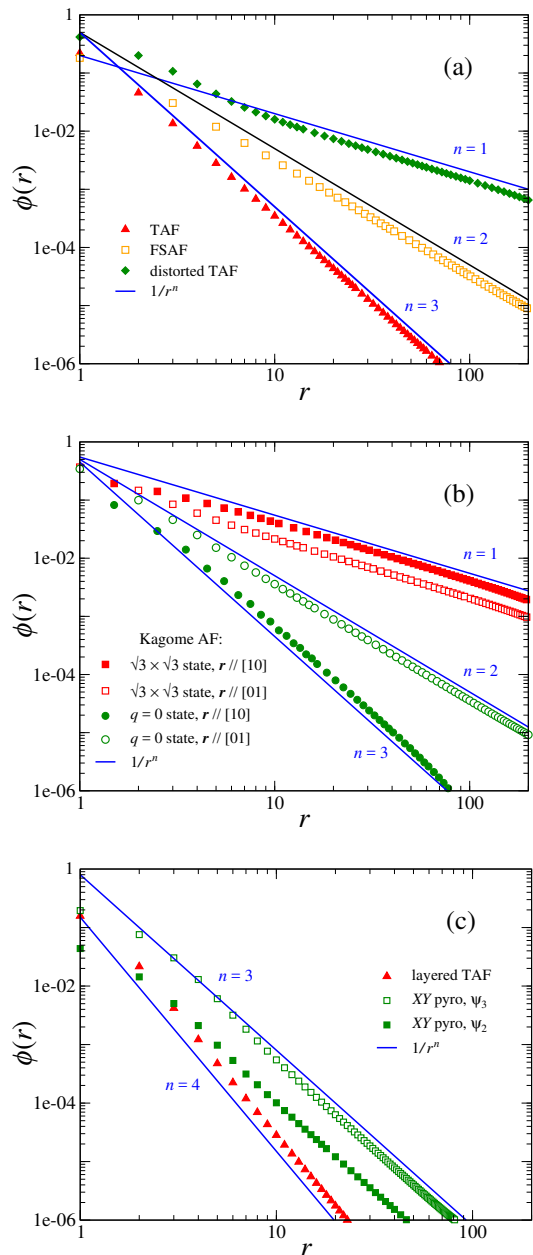


FIG. 2. Distortion angle ϕ versus distance for a vacancy in coplanar magnetic states. 2D models: (a) the triangular antiferromagnet (TAF), the frustrated square-lattice antiferromagnet (FSAFM), and the orthorhombically distorted TAF; (b) the J_1 - J_2 kagome antiferromagnet. 3D models: (c) the layered TAF and the XY pyrochlore antiferromagnets. The data points correspond to tilting angles in a relaxed state obtained numerically for a specific ordered spin structure in the presence of a lattice defect.

tortions obey Eq. (15) at large-distances with the $n = 4$ power-law exponent. Presented numerical results correspond to a spin chain along the [100] direction. These are full agreement with the analytic asymptote.

The second 3D model is a pyrochlore antiferromagnet with magnetic moments restricted to the local XY

planes that are orthogonal the trigonal axis at each site. This model has been widely investigated in relation to $\text{Er}_2\text{Ti}_4\text{O}_7$ and other rare-earth pyrochlores. We refer the interested reader to [33, 66] for further detailed discussion and notations of this interesting model. Depending on the ratio of two microscopic coupling constants, J_\perp and J_\perp^a , the quantum fluctuations choose either the noncoplanar state ψ_2 ($J_\perp^a/J_\perp < 4$) or the coplanar structure ψ_3 as the ground state ($J_\perp^a/J_\perp > 4$) [66], whereas the structural disorder in the form vacancies or bond defects has an opposite effect [33].

The theoretical consideration developed in the previous Subsection for the coplanar magnetic structures applies here as well since deformation of a magnetic structure formed by the XY spins is still described by a scalar field: the tilting angle $\phi(\mathbf{r}_i)$ of a spin from its equilibrium orientation in the local easy plane. Figure 2(c) shows the decay of spin distortions on a chain passing through the vacancy in the ψ_2 state ($J_\perp^a/J_\perp = 6$) and in the ψ_3 state ($J_\perp^a/J_\perp = 1$). The numerical results are compatible with the power-law exponent $n = 3$ in both cases, which in turn implies the quadrupole source term (16). In 3D case it is less convenient to use a graphical construction similar to Fig. 1 in the derivation of the torque multipole moment. Instead one can use Eqs. (5) and (11) to find out that the torque source for both states has the quadrupole symmetry.

III. NONCOPLANAR SPIN TEXTURES

A. Analytic Theory

The preceding analysis can be straightforwardly generalized to noncoplanar magnetic structures. Such spin arrangements can appear in various frustrated spin models, especially in the presence of structural disorder, which tends to stabilize the least collinear states [27, 32]. Specifically, we consider Heisenberg antiferromagnetic models on a face-centered cubic and on a pyrochlore lattices. We explore the energetics of ‘small deformations’ around the lowest-energy state defined by the zero-torque condition:

$$\mathbf{S}_i^0 \times \mathbf{h}_i = 0, \quad \mathbf{h}_i = - \sum_j J_{ij} \mathbf{S}_j^0. \quad (18)$$

This constraint is equivalent the condition that a spin is co-aligned with its molecular field. The spin deformation is described by a rotation matrix $\hat{\mathbf{R}}_i$ parametrized by a rotation axis \mathbf{n}_i and a rotation angle ϕ_i . Using the Euler-Rodrigues formula one can write for small ϕ_i :

$$\hat{\mathbf{R}}_i \mathbf{S}_i^0 = \mathbf{S}_i^0 + \phi_i \times \mathbf{S}_i^0 + \frac{1}{2} \phi_i \times (\phi_i \times \mathbf{S}_i^0), \quad (19)$$

where the vector field $\phi_i = \phi_i \mathbf{n}_i$ describes deformations of the magnetic structure. A generalization of the defor-

mation energy (6) to the noncoplanar case is

$$E_2 = -\frac{1}{2} \sum_{\langle ij \rangle} J_{ij} \left[(\mathbf{S}_i^0 \cdot \mathbf{S}_j^0) |\phi_i - \phi_j|^2 - (\phi_j \cdot \mathbf{S}_j^0) (\phi_j \cdot \mathbf{S}_i^0) - (\phi_i \cdot \mathbf{S}_i^0) (\phi_i \cdot \mathbf{S}_j^0) + 2(\phi_i \cdot \mathbf{S}_j^0) (\phi_j \cdot \mathbf{S}_i^0) \right]. \quad (20)$$

The last three terms in (20) provide the difference between the coplanar and the noncoplanar cases. These terms vanish in the coplanar case, whereas for a noncoplanar state they produce coupling between components of the deformation field ϕ .

Assuming that ϕ_i is a slowly varying field $\phi(\mathbf{r})$, which is true at large distances, we obtain the continuum description

$$E_2 \approx \frac{1}{2} \int d^D \mathbf{r} C_{\alpha\beta}^{ab} (\partial_\alpha \phi^a) (\partial_\beta \phi^b) \quad (21)$$

where, the elastic constants are expressed as

$$C_{\alpha\beta}^{ab} = -\frac{1}{\Omega} \sum_{i,j} J_{ij} (\ell_{ij})_\alpha (\ell_{ij})_\beta \left[(\mathbf{S}_i^0 \cdot \mathbf{S}_j^0) \delta^{ab} - \frac{1}{2} ((S_i^0)^a (S_j^0)^b + (S_j^0)^a (S_i^0)^b) \right]. \quad (22)$$

The summation is performed over sites in a magnetic unit cell, Ω is the cell volume, ℓ_{ij} are intersite distances, α, β are indices in the real space, and a, b are indices in the spin space. Note that when the ground state is non-coplanar, the different components ϕ^a are coupled to each other.

The presence of a vacancy in this system can be modeled as a source term in Eq. (21). The large-distance behavior of the spin deformations about a vacancy can again be predicted from the properties of Green’s function of the elasticity theory. Thus, for a delta function source located at the origin, we expect, in spatial dimension D

$$|\phi(r)| \sim \frac{1}{r^{D-2}} \quad (23)$$

For a source that has a leading multipole M , we expect the leading term to be

$$|\phi(r)| \sim \frac{1}{r^{D+M-2}} \quad (24)$$

If the source has higher multiples than M , then one may observe faster decay along special directions where the contributions of the lowest multipole vanishes owing to symmetry similar to the discussion in Sec. IIA for the $\sqrt{3} \times \sqrt{3}$ state in KAF.

B. Numerical results

The above theory is verified for the two classical models with noncoplanar magnetic structures: the nearest-neighbor Heisenberg antiferromagnets on fcc and pyrochlore lattices. The starting point is the linear equation

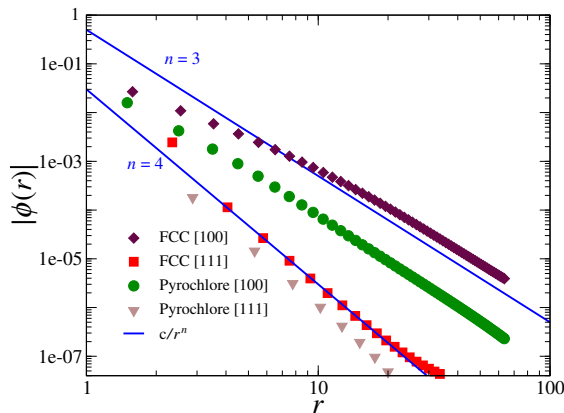


FIG. 3. Distortion angle ϕ versus distance around a vacancy in fcc and pyrochlore antiferromagnets with the all-in-all-out noncoplanar states. Numerical results are obtained by minimization of energy (20) using a periodic box with the linear size $L = 256$. [100] and [111] are the chosen crystallographic directions.

on ϕ_i obtained by variation of the quadratic energy (20) supplied with a source term produced by a vacancy. We numerically solve the resulting equation with the Fourier transform method.

Figure 3 shows the behavior of spin deformation fields in fcc and pyrochlore antiferromagnets induced by a vacancy. The ground state is the all-out state in both cases. The pyrochlore case has a large ground state degeneracy [67]. The spin deformation in this case is defined around the all out state, with possible zero energy local deformations. We find that along a generic direction, the spin deformation field decays as $1/r^3$. Further, along special directions (e.g., the [111] direction) we see a faster decay of $1/r^4$. These results are readily understood from the theory developed earlier. The vacancy induces source terms on the neighbor sites. Figure 4 shows the distribution of these source terms near a vacancy. In this case (and also for the fcc), we see that the lowest nonvanishing multipole moment of this source term is the quadrupole moment, i.e., the long distance behavior from Eq. (24) is indeed $1/r^3$ as found in numerical calculation. Further, the quadrupole field vanishes along certain directions; along these directions the octupole moment of the source term produces an $M = 3$, i.e., a $1/r^4$ decay of the spin deformation.

IV. DEFECT INDUCED MOMENTS

A removal of one spin from an antiferromagnetic crystal leaves an uncompensated magnetic moment. For non-collinear magnetic structures the resulting net moment is additionally screened by an induced spin texture [53]. Assuming that an impurity is located at $i = 1$, the total

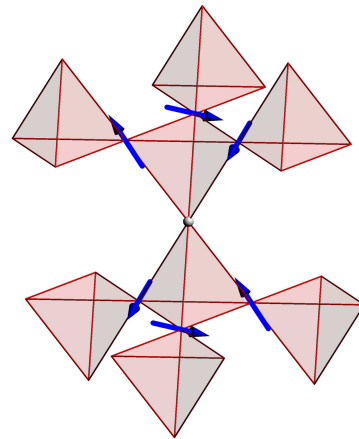


FIG. 4. Distribution source terms due to a vacancy in the pyrochlore antiferromagnet. The vacancy is indicated by a missing site, and the blue vectors indicate the source terms (uncompensated local magnetic field crossed with the local spin) induced by the missing site. The lowest vanishing multipole moment is the quadrupole moment.

moment can be written as

$$\mathbf{m}_{\text{imp}} = \sum_{i \neq 1} \mathbf{S}_i = \sum_{i \neq 1} \mathbf{m}_i - \mathbf{S}_1^{(0)}. \quad (25)$$

The last form is independent of the boundary conditions and can be used for commensurate as well as for incommensurate states. Generally, the moment m_{imp} has a nonuniversal fractional value, which needs to be determined numerically. The direction of \mathbf{m}_{imp} is, however, fixed by the background magnetic structure and in the absence of further symmetry breaking is locked to the direction of the missing spin $\mathbf{S}_1^{(0)}$.

The vacancy moments manifest themselves as the low-temperature Curie tail in the magnetic susceptibility

$$\chi_{\text{imp}} \simeq \frac{N_{\text{imp}} m_{\text{imp}}^2}{3T}, \quad (26)$$

where N_{imp} is a number of nonmagnetic impurities in the crystal [53, 56]. The effect is present for both 2D and 3D magnets irrespective of an ordering transition in the later case. Despite apparent similarity with the result for a paramagnet consisting of N_{imp} independent moments, Eq. (26) has a somewhat different meaning. As we explained before, the vacancy moments are locked to the specific sublattice directions in the ordered magnetic structure and do not fluctuate. Since random vacancies appear with equal probability on each of the antiferromagnetic sublattices, their total moment vanishes $\langle M_{\text{imp}} \rangle = 0$ for $N_{\text{imp}} \gg 1$. However, the average square moment remains nonzero and scales as $\langle M_{\text{imp}}^2 \rangle \approx N_{\text{imp}} m_{\text{imp}}^2$. It is this moment induced by configurational fluctuations which contributes to the low-temperature singularity in the magnetic susceptibility (26).

TABLE I. Magnetic moments induced by vacancies in various 2D and 3D models. Defect (impurity) bond results with $J_{\text{imp}} \neq J$ are also included for TAF.

Model	Parameters	M_{imp}/S	Power law
TAF, vacancy		-0.03974	$1/r^3$
TAF, bond	$J_{\text{imp}} = 0.5J$	0.19383	$1/r$
	$J_{\text{imp}} = -0.5J$	0.52928	$1/r$
FSAF	$J_2/J_1 = 1$	0.50289	$1/r^2$
FSAF	$J_2/J_1 = 0.7$	0.29232	$1/r^2$
KAF	$J_2/J_1 = 0.1$	-0.04242	$1/r^2$
	$J_2/J_1 = -0.1$	-0.02719	$1/r$
distorted TAF	$J'/J = 0.765$	0.04398	$1/r$
	$J'/J = 0.518$	0.25827	$1/r$
layered TAF	$J_c/J = 1$	0.43213	$1/r^4$
	$J_c/J = 0.1$	0.03969	$1/r^4$

Let us now consider how the different decay laws for spin textures affect the vacancy moment (25). In particular, the important question is if the dipole-like deformation field gives finite or diverging contributions from large distances. For concreteness, we consider a distorted incommensurate spiral

$$\mathbf{S}_i = (\sin(\mathbf{Q} \cdot \mathbf{r}_i + \phi_i), 0, \cos(\mathbf{Q} \cdot \mathbf{r}_i + \phi_i)) \quad (27)$$

with ϕ_i obeying Eq. (14). Then, the magnetic moment of the spin texture is approximately given by

$$\delta m_{\text{imp}}^z = - \sum_i \frac{\mathbf{d} \cdot \mathbf{r}_i}{r_i^D} \sin(\mathbf{Q} \cdot \mathbf{r}_i). \quad (28)$$

Replacing the lattice sum by a space integral we obtain in 2D for the contribution accumulated at large distances $r > a^*$:

$$\begin{aligned} \delta m_{\text{imp}}^z &= -d \iint \frac{dx dy}{V_0} \frac{x \sin Qx}{x^2 + y^2} \\ &= -d \int_{a^*}^{\infty} \frac{dr}{V_0} \int_0^{2\pi} d\varphi \cos \varphi \sin(Qr \cos \varphi) \\ &= -2\pi d \int_{a^*}^{\infty} \frac{dr}{V_0} J_1(Qr) = -\frac{2\pi d}{V_0 Q} J_0(Qa^*), \end{aligned} \quad (29)$$

where d is the dipole moment of the spin distortion field, V_0 is the unit cell volume, and $J_0(x)$, $J_1(x)$ are the two Bessel functions. Thus, the long-range contribution to m_{imp} remains finite. This conclusion can be easily extended to 3D and to other types of the magnetic deformation fields (15) and (16).

Table I presents numerical values for the vacancy moments in a few selected spin models. Positive or negative value of the moment corresponds to whether it is antiparallel or parallel to the missing spin $\mathbf{S}_1^{(0)}$. In a collinear magnetic state, the vacancy moment is equal to $-\mathbf{S}_1^{(0)}$ and, hence, is positive according to the above definition. In TAF the missing spin is overscreened by the

induced spin texture such that the moment becomes negative [53]. The sign change is also present for vacancies in KAF, where spin textures exhibit a different large-distance behavior from TAF. Hence, underscreening or overscreening is mostly produced by local spin canting in a few nearest-neighbor shells around the impurity.

As has been discussed in Sec. II, a defect bond also generates the dipole type spin texture (14). Hence, a finite value of the lattice sum in Eq. (28) signifies that defect bonds in noncollinear antiferromagnets must also produce uncompensated magnetic moments. Their direction is now fixed by the sum of two spins on each defect bond and the fractional values can widely vary. To our knowledge this effect has not been so far discussed in the literature on structural defects. For illustration, we compute and present in Table I the values of magnetic moments associated with a defect bond $J_{\text{imp}} \neq J$ in TAF for two values of J_{imp} . Note, that the model of defect bonds in TAF is relevant to the triangular antiferromagnet $\text{RbFe}(\text{MoO}_4)_2$ for which nonmagnetic substitution of Rb by K introduces random modulations of exchange bonds between iron ions [8].

V. DISCUSSION

We have presented a comprehensive theoretical analysis of spin textures induced by lattice defects, in particular, nonmagnetic vacancies, in ordered noncollinear magnets. Our results explain the apparently conflicting results in the literature about the exponent of the power-law tail in the distance dependence of vacancy induced spin distortions [39, 53, 54]. Besides space dimension, the corresponding power-law exponent is determined, by symmetry of the torque, which in turn depends on the magnetic structure. Perhaps the most striking example of this conclusion is provided by the $q = 0$ and the $\sqrt{3} \times \sqrt{3}$ states, on a kagome lattice. Both states have locally the same 120° magnetic structure albeit with different arrangements of spin chiralities. Such a difference leads to different decay laws of the spin distortions: $1/r^2$ ($q = 0$) and $1/r$ ($\sqrt{3} \times \sqrt{3}$).

The developed elastic-type theory is inherently concerned with the long-wavelength physics. While input from the lattice scale is important and useful, such in the case of determining the multipolar nature of a defect mentioned above, our theory yields the long-distance asymptotics and not necessarily the full quantitative form of the distortion at short distances.

The above consideration can be straightforwardly extended to other types of structural defects and associated perturbations in the spin Hamiltonians. These may include magnetic impurities or add-on spins, locally modified spin-orbit coupling as, for example, the Dzyaloshinskii-Moriya term [59] and so on. Similar to the problem of an antiferromagnetic bond in a collinear ferromagnet [20–23], in some of these cases an additional symmetry lowering can be expected once the strength of

a local perturbation exceeds a critical value.

Our single-impurity results have important consequence for the interaction between impurities, and thus their eventual behavior at finite impurity concentration. Our elastic theory implies long-range interactions mediated by the induced spin distortions. As a consequence, longer-range tails in the induced spin distortions should lead to fragile magnetic phases and faster transformation into a disordered spin-glass like state upon doping with nonmagnetic impurities. It will be interesting to perform direct numerical studies of such effects.

Finally, an interesting direction concerns interplay and competition between thermal and quantum fluctuations and the response to vacancies in the many classical ground states in frustrated magnets which are degenerate but not symmetry-related. While competing tendencies

of fluctuation- and disorder-induced ordering have been known for a long time [27], we are not aware of a comprehensive study of all the possible combinations of unperturbed states and disorder types for determining the eventual low-temperature behavior of such magnets.

ACKNOWLEDGMENTS

We thank M. Vojta for discussions. M.E.Z. acknowledges support from the ANR, France, Grant No. ANR-19-CE30-0040. V. B. S. thanks SERB, DST, India for support. This work was supported in part by the Deutsche Forschungsgemeinschaft under Grant No. SFB 1143 (Project-ID No. 247310070) and by the Deutsche Forschungsgemeinschaft under cluster of excellence ct.qmat (EXC 2147, Project-ID No. 390858490).

-
- [1] J. Bobroff, N. Laflorencie, L. K. Alexander, A. V. Mahajan, B. Koteswararao, and P. Mendels, Impurity-Induced Magnetic Order in Low-Dimensional Spin-Gapped Materials, *Phys. Rev. Lett.* **103**, 047201 (2009).
- [2] S. E. Dutton, C. L. Broholm, and R. J. Cava, Divergent effects of static disorder and hole doping in geometrically frustrated β -CaCr₂O₄, *J. Solid State Chem.* **183**, 1798 (2010).
- [3] T. Okuda, K. Uto, S. Seki, Y. Onose, Y. Tokura, R. Kajimoto, and M. Matsuda, Effect of Spin Dilution on the Magnetic State of Delafossite CuCrO₂ with an $S = 1/2$ Antiferromagnetic Triangular Sublattice, *J. Phys. Soc. Jpn.* **80**, 014711 (2011).
- [4] G. Simutis, S. Gvasaliya, M. Månsson, A. L. Chernyshev, A. Mohan, S. Singh, C. Hess, A. T. Savici, A. I. Kolesnikov, A. Piovano, T. Perring, I. Zaliznyak, B. Büchner, and A. Zheludev, Spin Pseudogap in Ni-Doped SrCuO₂, *Phys. Rev. Lett.* **111**, 067204 (2013).
- [5] J. W. Kim, Y. Kamiya, E. D. Mun, M. Jaime, N. Harrison, J. D. Thompson, V. Kiryukhin, H. T. Yi, Y. S. Oh, S.-W. Cheong, C. D. Batista, and V. S. Zapf, Multiferroicity with coexisting isotropic and anisotropic spins in Ca₃Co_{2-x}Mn_xO₆, *Phys. Rev. B* **89**, 060404(R) (2014).
- [6] J. F. Niven, M. B. Johnson, A. Bourque, P. J. Murray, D. D. James, H. A. Dąbkowska, B. D. Gaulin, and M. A. White, Magnetic phase transitions and magnetic entropy in the XY antiferromagnetic pyrochlores (Er_{1-x}Y_x)₂Ti₂O₇, *Proc. R. Soc. A* **470**, 20140387 (2014).
- [7] K. A. Ross, J. W. Krizan, J. A. Rodriguez-Rivera, R. J. Cava, and C. L. Broholm, Static and dynamic XY-like short-range order in a frustrated magnet with exchange disorder, *Phys. Rev. B* **93**, 014433 (2016).
- [8] A. I. Smirnov, T. A. Soldatov, O. A. Petrenko, A. Takata, T. Kida, M. Hagiwara, A. Ya. Shapiro, and M. E. Zhitomirsky, Order by Quenched Disorder in the Model Triangular Antiferromagnet RbFe(MoO₄)₂, *Phys. Rev. Lett.* **119**, 047204 (2017).
- [9] A. Orlova, H. Mayaffre, S. Krämer, M. Dupont, S. Capponi, N. Laflorencie, A. Paduan-Filho, M. Horvatić, Detection of a Disorder-Induced Bose-Einstein Condensate in a Quantum Spin Material at High Magnetic Fields, *Phys. Rev. Lett.* **121**, 177202 (2018).
- [10] I. Mirebeau, N. Martin, M. Deutsch, L. J. Bannenberg, C. Pappas, G. Chaboussant, R. Cubitt, C. Decorse, and A. O. Leonov, Spin textures induced by quenched disorder in a reentrant spin glass: Vortices versus “frustrated” skyrmions. *Phys. Rev. B* **98**, 014420 (2018).
- [11] D. F. Bowman, E. Cemal, T. Lehner, A. R. Wildes, L. Mangin-Thro, G. J. Nilsen, M. J. Gutmann, D. J. Vonshen, D. Prabhakaran, A. T. Boothroyd, D. G. Porter, C. Castelnovo, K. Refson, and J. P. Goff, Role of defects in determining the magnetic ground state of ytterbium titanate, *Nature Commun.* **10**, 637 (2019).
- [12] S. Lim, S. Park, S. Lee, K. Park, H. Sim, J.-G. Park, S. Lee, and H. E. Maynard-Casely, Spin-disorder state near nonmagnetic impurities in the frustrated antiferromagnet YMnO₃, *Phys. Rev. B* **102**, 184427 (2020).
- [13] L. Facheris, D. Blosser, K. Y. Povarov, R. Bewley, S. Gvasaliya, A. Zheludev, Finite-temperature dynamics and the role of disorder in nearly critical Ni(Cl_{1-x}Br_x)₂·4SC(NH₂)₂, *Phys. Rev. B* **102**, 224405 (2020).
- [14] C. Pughe, O. H. J. Mustonen, A. S. Gibbs, S. Lee, R. Stewart, B. Gade, C. Wang, H. Luetkens, A. Foster, F. C. Coomer, H. Takagi, E. J. Cussen, Partitioning the Two-Leg Spin Ladder in Ba₂Cu_{1-x}Zn_xTeO₆: From Magnetic Order through Spin-Freezing to Paramagnetism, *Chem. Mater.* **35**, 2752 (2023).
- [15] B. D. S. Chandana, A. Narayanan, K. Saranya, D. C. Kakarla, A. Tiwari, B. Shanmugavelu, G. Peramaiyan, G. C. Shekar, K. Y. Choi, I. P. Muthuselvam, Magnetic order induced by magnetic impurities in the Haldane chain compound SrNi₂V₂O₈, *J. Magn. Magn. Mater.* **603**, 172219 (2024).
- [16] T. Jungwirth, J. Wunderlich, V. Novak, K. Olejnik, B. L. Gallagher, R. P. Campion, K. W. Edmonds, A. W. Rushforth, A. J. Ferguson, and P. Němec, Spin-dependent phenomena and device concepts explored in (Ga,Mn)As, *Rev. Mod. Phys.* **86**, 855 (2014).
- [17] T. Dietl, K. Sato, T. Fukushima, A. Bonanni, M. Jamet, A. Barski, S. Kuroda, M. Tanaka, P. N. Hai, and H. Katayama-Yoshida, Spinodal nanodecomposition in semiconductors doped with transition metals, *Rev. Mod. Phys.* **86**, 855 (2014).

- Phys. **87**, 1311 (2015).
- [18] M. Morin, E. Canévet, A. Raynaud, M. Bartkowiak, D. Sheptyakov, V. Ban, M. Kenzelmann, E. Pomjakushina, K. Conder, M. Medarde, *Nature Commun.* **7**, 13758 (2016).
- [19] P.-G. de Gennes, Canted Spin Arrangements, *Phys. Rev. Lett.* **3**, 209 (1959).
- [20] J. Villain, Insulating Spin Glasses, *Z. Phys. B* **33**, 31 (1979).
- [21] A. Aharony, R. J. Birgeneau, A. Coniglio, M. A. Kastner, and H. E. Stanley, Magnetic phase diagram and magnetic pairing in doped La_2CuO_4 , *Phys. Rev. Lett.* **60**, 1330 (1988).
- [22] G. N. Parker and W. M. Saslow, Defect interactions and canting in ferromagnets, *Phys. Rev. B* **38**, 11718 (1988).
- [23] J. Vannimenus, S. Kirkpatrick, F. D. M. Haldane, and C. Jayaprakash, Ground-state morphology of random frustrated XY systems, *Phys. Rev. B* **39**, 4634 (1989).
- [24] P. Gawiec and D. R. Grempel, Numerical study of the ground-state properties of a frustrated XY model, *Phys. Rev. B* **44**, 2613 (1991).
- [25] L. I. Glazman and A. S. Iosevich, Theory of the reentrant transition in a lamellar antiferromagnet: doped La_2CuO_4 , *Z. Phys. B* **80**, 133 (1990).
- [26] D. N. Aristov and S. V. Maleyev, Quantum frustrations in quasi-2D antiferromagnets, *Z. Phys. B* **81**, 433 (1990).
- [27] C. L. Henley, Ordering due to disorder in a frustrated vector antiferromagnet, *Phys. Rev. Lett.* **62**, 2056 (1989).
- [28] M. W. Long, Effects that can stabilise multiple spin-density waves, *J. Phys. Condens. Matter* **1**, 2857 (1989).
- [29] J. C. Slonczewski, Fluctuation mechanism for biquadratic exchange coupling in magnetic multilayers, *Phys. Rev. Lett.* **67**, 3172 (1991).
- [30] Y. V. Fyodorov and E. F. Shender, Random-field effects in antiferromagnets with classically degenerate ground states, *J. Phys. Condens. Matter* **3**, 9123 (1991).
- [31] L. Savary, E. Gull, S. Trebst, J. Alicea, D. Bergman, and L. Balents, Impurity effects in highly frustrated diamond-lattice antiferromagnets, *Phys. Rev. B* **84**, 064438 (2011).
- [32] V. S. Maryasin and M. E. Zhitomirsky, Triangular Antiferromagnet with Nonmagnetic Impurities, *Phys. Rev. Lett.* **111**, 247201 (2013).
- [33] V. S. Maryasin and M. E. Zhitomirsky, Order from structural disorder in the XY pyrochlore antiferromagnet $\text{Er}_2\text{Ti}_2\text{O}_7$, *Phys. Rev. B* **90**, 094412 (2014).
- [34] A. Andreanov and P. A. McClarty, Order induced by dilution in pyrochlore XY antiferromagnets, *Phys. Rev. B* **91**, 064401 (2015).
- [35] L. Bellier-Castella, M. J. P. Gingras, P. C. W. Holdsworth, and R. Moessner, Frustrated order by disorder: The pyrochlore anti-ferromagnet with bond disorder, *Can. J. Phys.* **79**, 1365 (2001).
- [36] T. E. Saunders and J. T. Chalker, Spin Freezing in Geometrically Frustrated Antiferromagnets with Weak Disorder, *Phys. Rev. Lett.* **98**, 157201 (2007).
- [37] A. Andreanov, J. T. Chalker, T. E. Saunders, and D. Sherrington, Spin-glass transition in geometrically frustrated antiferromagnets with weak disorder, *Phys. Rev. B* **81**, 014406 (2010).
- [38] E. C. Andrade, J. A. Hoyos, S. Rachel, and M. Vojta, Cluster-Glass Phase in Pyrochlore XY Antiferromagnets with Quenched Disorder, *Phys. Rev. Lett.* **120**, 097204 (2018).
- [39] C. L. Henley, Effective Hamiltonians and dilution effects in Kagome and related anti-ferromagnets, *Can. J. Phys.* **79**, 1307 (2001).
- [40] J. Rehn, A. Sen, A. Andreanov, K. Damle, R. Moessner, and A. Scardicchio, Random Coulomb antiferromagnets: From diluted spin liquids to Euclidean random matrices, *Phys. Rev. B* **92**, 085144 (2015).
- [41] L. Savary and L. Balents, Disorder-Induced Quantum Spin Liquid in Spin Ice Pyrochlores, *Phys. Rev. Lett.* **118**, 087203 (2017).
- [42] T. Bilitewski, M. E. Zhitomirsky, and R. Moessner, Jammed Spin Liquid in the Bond-Disordered Kagome Antiferromagnet, *Phys. Rev. Lett.* **119**, 247201 (2017).
- [43] I. Kimchi, A. Nahum, T. Senthil, Valence Bonds in Random Quantum Magnets: Theory and Application to YbMgGaO_4 , *Phys. Rev. X* **8**, 031028 (2018).
- [44] P. M. Consoli and M. Vojta, Disorder effects in spiral spin liquids: Long-range spin textures, Friedel-like oscillations, and spiral spin glasses, *Phys. Rev. B* **109**, 064423 (2024).
- [45] M. Sigrist and A. Furusaki, Low-Temperature Properties of the Randomly Depleted Heisenberg Ladder, *J. Phys. Soc. Jpn.* **65**, 2385 (1996).
- [46] P. Schiffer and I. Daruka, Two-population model for anomalous low-temperature magnetism in geometrically frustrated magnets, *Phys. Rev. B* **56**, 13712 (1997).
- [47] R. Moessner and A. J. Berlinsky, Magnetic Susceptibility of Diluted Pyrochlore and $\text{SrCr}_{9-9x}\text{Ga}_{3+9x}\text{O}_{19}$ Antiferromagnets, *Phys. Rev. Lett.* **83**, 3293 (1999).
- [48] S. Sachdev, C. Buragohain, and M. Vojta, Quantum Impurity in a Nearly Critical Two-Dimensional Antiferromagnet, *Science* **286**, 2479 (1999).
- [49] S. Sachdev and M. Vojta, Quantum impurity in an antiferromagnet: Nonlinear sigma model theory, *Phys. Rev. B* **68**, 064419 (2003).
- [50] K. H. Höglund, A. W. Sandvik, and S. Sachdev, Impurity Induced Spin Texture in Quantum Critical 2D Antiferromagnets, *Phys. Rev. Lett.* **98**, 087203 (2007).
- [51] S. Eggert, O. F. Syljuåsen, F. Anfuso, and M. Andres, Universal Alternating Order around Impurities in Antiferromagnets, *Phys. Rev. Lett.* **99**, 097204 (2007).
- [52] A. Sen, K. Damle, and R. Moessner, Fractional Spin Textures in the Frustrated Magnet $\text{SrCr}_{9p}\text{Ga}_{12-9p}\text{O}_{19}$, *Phys. Rev. Lett.* **106**, 127203 (2011).
- [53] A. Wollny, L. Fritz, and M. Vojta, Fractional Impurity Moments in Two-Dimensional Noncollinear Magnets, *Phys. Rev. Lett.* **107**, 137204 (2011).
- [54] C. Weber and F. Mila, Anticollinear magnetic order induced by impurities in the frustrated Heisenberg model of pnictides, *Phys. Rev. B* **86**, 184432 (2012).
- [55] A. Sen, K. Damle, and R. Moessner, Vacancy-induced spin textures and their interactions in a classical spin liquid, *Phys. Rev. B* **86**, 205134 (2012).
- [56] V. S. Maryasin and M. E. Zhitomirsky, Collective impurity effects in the Heisenberg triangular antiferromagnet, *J. Phys.: Conf. Series* **592**, 012112 (2015).
- [57] O. I. Utesov, A. V. Sizanov, A. V. Syromyatnikov, Spiral magnets with Dzyaloshinskii-Moriya interaction containing defect bonds, *Phys. Rev. B* **92**, 125110 (2015).
- [58] S.-Z. Lin, S. Hayami, and C. D. Batista, Magnetic Vortex Induced by Nonmagnetic Impurity in Frustrated Magnets, *Phys. Rev. Lett.* **116**, 187202 (2016).
- [59] S. Hayami, H. Kusunose, and Y. Motome, Magnetic Vortex Induced by Nonmagnetic Impurity in Ferromagnets:

- Magnetic Multipole and Toroidal around the Vacancy, *J. Phys. Soc. Jpn.* **88**, 063702 (2019).
- [60] S. Maekawa, H. Adachi, K. Uchida, J. Ieda, and E. Saitoh, Spin Current: Experimental and Theoretical Aspects, *J. Phys. Soc. Jpn.* **82**, 102002 (2013).
- [61] L. Messio, C. Lhuillier, and G. Misguich, Lattice symmetries and regular magnetic orders in classical frustrated antiferromagnets, *Phys. Rev. B* **83**, 184401 (2011).
- [62] S. Katsura, T. Morita, S. Inawashiro, T. Horiguchi, and Y. Abe, Lattice Green's Function. Introduction, *J. Math. Phys.* **12**, 892 (1971).
- [63] J. T. Chalker, P. C. W. Holdsworth, and E. F. Shender, Hidden Order in a Frustrated System: Properties of the Heisenberg Kagome Antiferromagnet, *Phys. Rev. Lett.* **68**, 855 (1992).
- [64] A. B. Harris, C. Kallin, and A. J. Berlinsky, Possible Néel orderings of the Kagomé antiferromagnet, *Phys. Rev. B* **45**, 2899 (1992).
- [65] I. Ritchey, P. Chandra, and P. Coleman, Spin folding in the two-dimensional Heisenberg kagome antiferromagnet, *Phys. Rev. B* **47**, 15342 (1993).
- [66] M. E. Zhitomirsky, M. V. Gvozdkova, P. C. W. Holdsworth, and R. Moessner, Quantum Order by Disorder and Accidental Soft Mode in $\text{Er}_2\text{Ti}_2\text{O}_7$, *Phys. Rev. Lett.* **109**, 077204 (2012).
- [67] R. Moessner, and J. T. Chalker, Low-temperature properties of classical geometrically frustrated antiferromagnets, *Phys. Rev. B* **58**, 12049 (1998).